New high precision U-Pb ages and Hf isotope data from the Karoo large igneous province; implications for pulsed magmatism and early Toarcian environmental perturbations

Nicolas Greber, Joshua H.F.L. Davies, Sean Gaynor, Fred Jourdan, Hervé Bertrand, Urs Schaltegger

Results in Geochemistry 1 (2020) 100005

Contents lists available at ScienceDirect

Results in Geochemistry

journal homepage: www.elsevier.com/locate/ringeo

Research Paper

New high precision U-Pb ages and Hf isotope data from the Karoo large igneous province; implications for pulsed magmatism and early Toarcian environmental perturbations

Nicolas D. Greber[a,b,*], Joshua H.F.L. Davies[b,c], Sean P. Gaynor[b], Fred Jourdan[d], Hervé Bertrand[e], Urs Schaltegger[b]

[a] Institute of Geological Sciences, University of Bern, 3012 Bern, Switzerland
[b] Department of Earth Sciences, University of Geneva, 1205 Geneva, Switzerland
[c] Département des Sciences de la Terre et de l'Atmosphère, Université du Québec à Montréal, Montréal Québec H3C 3P8, Canada
[d] Western Australian Argon Isotope Facility, School of Earth and Planetary Sciences and JdL Centre, Curtin University, Perth, WA 6845, Australia
[e] Univ Lyon, ENSL, Univ Lyon 1, CNRS, LGL-TPE, F-69007 Lyon, France

ARTICLE INFO

Keywords:
Karoo
Large Igneous Province
Pliensbachian
Toarcian
U-Pb
40Ar/39Ar

ABSTRACT

To better constrain the age and duration of the magmatism associated with the Karoo large igneous province (LIP), we present new U-Pb ID-TIMS dates and εHf values from baddeleyite and zircon grains from Karoo basin mafic sills and from felsic samples from the Lebombo and Mwenezi monoclines, together with an $^{40}Ar/^{39}Ar$ age database of Karoo rocks that has been filtered for true plateau ages with >70% of ^{39}Ar released and in which all $^{40}Ar/^{39}Ar$ ages were recalculated using the current best estimates for the decay constants. Zircon and baddeleyite ages from three Karoo basin sills range from 183.36 ± 0.17/0.27 to 183.06 ± 0.07/0.21 Ma, where the two uncertainties reflect the analytical error and the additional error associated with decay constant uncertainty. Zircon from the Mutandawhe pluton are dated to 176.84 ± 0.06/0.20 Ma, which represents the first high-precision U-Pb age of the late stage Karoo-LIP magmatism in the northern Lebombo-Mwenezi region. Initial hafnium isotopes are close to chondritic for the Karoo basin and central Lebombo samples (εHf from −2 to +3), but more negative for zircon grains from the Mutandawhe pluton (−11.3 ± 1.1, 2SD). In combination with previous studies and in agreement with the updated $^{40}Ar/^{39}Ar$ ages, we show that the sill complex that intruded the Karoo basin was short-lived at ~320 ± 180 ka and that it pre-dated the magmatism of the Ferrar-LIP by around 460 ka, whereas the entire Karoo-LIP was emplaced over a period of ca. 6.5 Ma. Based on high-precision U-Pb geochronology, Karoo-LIP magmatism occurred after 183.36 ± 0.17 Ma and therefore postdated the extinction pulses of the late Pliensbachian and likely the Pliensbachian-Toarcian boundary. However, we support previous conclusions that the start of the Karoo-LIP activity agrees with the onset of the Toarcian oceanic anoxic event and the early Toarcian warming, indicating that these environmental changes were likely a response to the magmatic activity of the Karoo-LIP.

1. Introduction

Large igneous provinces (LIPs) typically consist of massive volumes of mafic lava flows and/or sills and dykes and occur apparently outside of normal plate tectonic processes (Bryan & Ernst, 2008). Even though their total lifespan can reach several million years, often, most material is emplaced in short pulses of less than one million years (Burgess et al., 2015, 2017; Davies et al., 2017; Kasbohm & Schoene, 2018). Emplaced magma volumes can reach millions of cubic-kilometers, and are associated with the release of volatiles to the atmosphere (e.g., CO_2, SO_2, HCl, HF) derived from magmatic degassing (Capriolo et al., 2020; Sobolev et al., 2011), contact metamorphism of sediments (Ganino & Arndt, 2009; Heimdal et al., 2020) or from volatile release of assimilated sediments (Heimdal et al., 2019). Large igneous provinces are therefore important occurrences in Earth history as they can cause major climatic disruption. However, apart from a few well studied cases, the duration of volcanic activity and the temporal link to global climate perturbations are often not precisely established.

The Karoo and Ferrar LIPs are spread over three modern continents: Africa, Antarctica and Australia (Storey et al., 2013). The Karoo-LIP was emplaced into and onto the Karoo basin in South Africa, Lesotho and Swaziland as well as further north in Zimbabwe, Mozambique,

* Corresponding author at: Institute of Geological Sciences, University of Bern, 3012 Bern, Switzerland.
E-mail addresses: greber@geo.unibe.ch, nicolas.greber@geo.unibe.ch (N.D. Greber).

https://doi.org/10.1016/j.ringeo.2020.100005
Received 3 August 2020; Received in revised form 2 October 2020; Accepted 13 October 2020

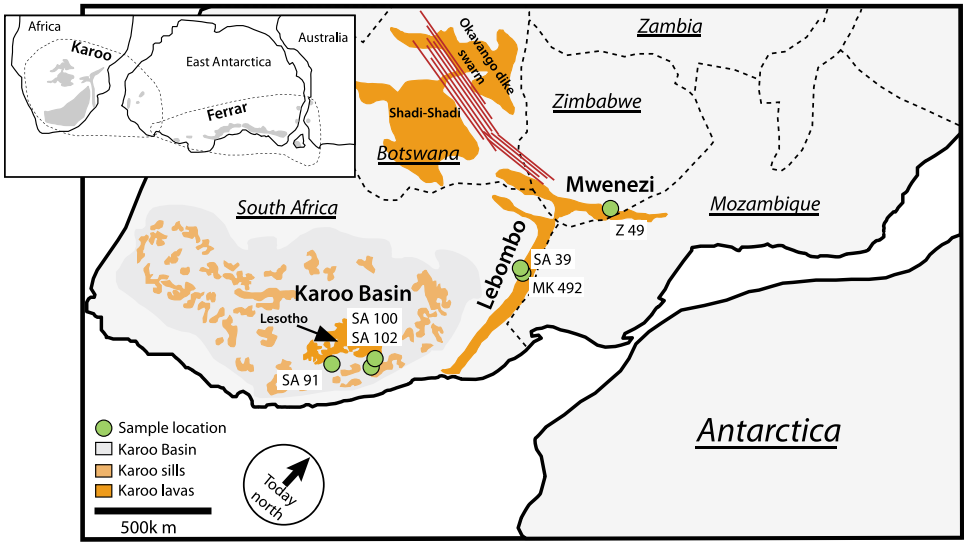

Fig. 1. Simplified overview of the Karoo-LIP during mid-Gondwana age following Luttinen (2018) with sample locations and naming of different regions. The inset illustrates the close geographical relationship between the Karoo and the Ferrar large igneous provinces.

Botswana, Zambia and westwards in Namibia (Bristow, 1982; Jourdan et al., 2007b; Sweeney et al., 1994) . A limited amount of outcrops also occur in western Antarctica (Riley et al., 2005). Activity related to the Ferrar-LIP, on the other hand, is found in Antarctica and Tasmania (Australia). Previous $^{40}Ar/^{39}Ar$ geochronology of the Karoo-LIP (Jourdan et al., 2005, 2007b, 2008) recently recalibrated to the ^{40}K constants proposed by Renne et al. (2011) and filtered for statistical quality by Ware et al. (2018) suggested that magmatic activity started at ~185 Ma and ceased ~176 Ma. It has also been proposed that the bulk of the Karoo-LIP magmatism was almost continuously emplaced over ~4.5 Ma (Jourdan et al., 2008) from ca. 184.0 Ma to 179.5 Ma (Ware et al., 2018). In contrast to the Karoo-LIP, U-Pb zircon ages from the Ferrar-LIP define a short emplacement interval in Antarctica (182.78 ± 0.03 to 182.43 ± 0.04 Ma) and Tasmania (182.90 ± 0.19 to 182.54 ± 0.06 Ma) (Burgess et al., 2015; Ivanov et al., 2017). Published U-Pb zircon ages for the Karoo-LIP are mostly restricted to the Karoo basin sill complex in the southern part of the Karoo-LIP (Fig. 1), and suggest a narrow time window of magmatism ranging from 183.246 ± 0.045 to 182.7 ± 0.6 Ma (Burgess et al., 2015; Corfu et al., 2016; Sell et al., 2014). The timing of emplacement of the sills of the Karoo basin is of major importance due to their possible connection to the negative carbon isotope excursion and associated environmental perturbations in the early Toarcian (Svensen et al., 2012). Furthermore, in total six periods of biotic disturbance and extinction have been recognized in the stratigraphic record between the early Pliensbachian and late Toarcian and all of these have been associated with the Karoo and Ferrar magmatic events (Caruthers et al., 2013; Dera et al., 2010). However, some of these disturbances occur before and after the early Toarcian carbon isotope excursion, as well as before and after the magmatism in the Karoo basin, rendering the relationships between the LIP, the biotic crises and carbon isotope excursions contentious (Caruthers et al., 2013; Gómez et al., 2008; Pálfy & Smith, 2000; Percival et al., 2015; Rita et al., 2019). In addition, no high precision U-Pb ages exist from the late silicic Karoo-LIP magmatism in the northern Mwenezi region (Zimbabwe-Mozambique border, see Fig. 1), which, based on the most precise $^{40}Ar/^{39}Ar$ ages occurred between 176.2 ± 0.7 and 179.0 ± 0.8 Ma (recalculated using the decay constants of Renne et al., 2011) and is used as marker for the end of the Karoo-LIP (Jourdan et al., 2007b).

In order to better constrain the timing of the Karoo-LIP in Southern Africa relative to the environmental disturbances, and also to confirm the presence and association of the younger silicic magmatism with the rest of the Karoo-LIP, we present new high-precision U-Pb isotope-dilution TIMS ages and εHf values of baddeleyite and zircon from rocks on a south to north transect of the Karoo-LIP.

2. Compilation of Karoo large igneous province ages; high-precision U-Pb and filtered $^{40}Ar/^{39}Ar$ data

To be able to better compare published $^{40}Ar/^{39}Ar$ ages with high-precisions U-Pb ages, we followed the method of Ware et al. (2018) and filtered the available $^{40}Ar/^{39}Ar$ data based on more stringent selection criteria using only true plateau ages with >70% of ^{39}Ar released and recalculated all $^{40}Ar/^{39}Ar$ ages using the decay constants of Renne et al. (2011) (see supplementary Tables S1 and S2). Furthermore, we only consider data from mineral separates; groundmass $^{40}Ar/^{39}Ar$ ages are not included in our database. Results from the following publication were used for the $^{40}Ar/^{39}Ar$ age Karoo-LIP database: Landoll et al. (1989), Duncan et al. (1997), Jones et al. (2001), Le Gall et al. (2002), Zhang et al. (2003), Jourdan et al. (2004, 2005, 2007b, 2007c, 2008), Riley et al. (2005, 2006), Luttinen et al. (2015), Moulin et al. (2017) and Ware et al. (2018).

Supplementary Table S3 presents a compilation of high-precision U-Pb zircon and baddeleyite ages normalized to the EARTHTIME U-Pb spike timeline from the Karoo-LIP and the Ferrar-LIP using data from Sell et al. (2014), Burgess et al. (2015), Corfu et al. (2016) and Ivanov et al. (2017).

3. Sample material and methods

3.1. Bulk grain high precision U–Pb dating by CA-ID-TIMS

We dated baddeleyite or zircon from three sills intruding the Beaufort group of the Karoo basin (SA91, SA100, SA102), one porphyritic rhyolite flow that was sampled at the Olifants river in the central Lebombo region (MK492), and a syenite from the Mutandawhe pluton in the Mwenezi area, Zimbabwe (Z49) (Fig. 1, coordinates are listed in supplementary Table S4). The three sill samples from the Beaufort group are coarse-grained gabbros. In samples SA100 and SA102 we found tabular-shaped and transparent, brown-reddish baddeleyite crystals, and from sample SA91 we were able to extract euhedral zircon grains. For the latter, Sell et al. (2014) already reported baddeleyite U-Pb ages ranging from 181.34 ± 0.12 to 182.69 ± 0.09 Ma. Rhyolite MK492 from the Lebombo contains abundant, transparent and euhedral zircon grains. The syenite from the Mutandawhe pluton (Z49) is located in the Mwenezi region and has previously been dated with $^{40}Ar/^{39}Ar$ to 176.2 ± 0.7 Ma (see Jourdan et al., 2007b and Table S2). It also contains euhedral zircon grains. Therefore, our samples define a S-to-N transect through the Karoo-LIP, including rocks associated with temporally dis-

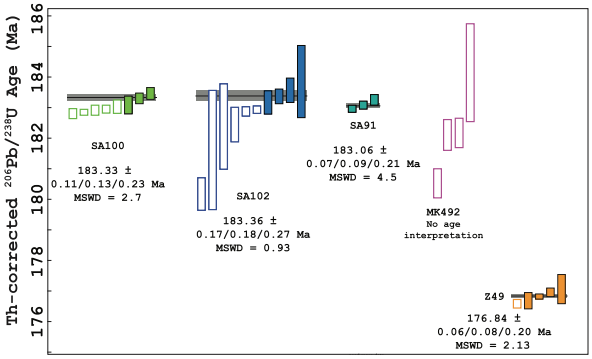

Fig. 2. Interpretation and weighted means of Th-corrected $^{206}Pb/^{238}U$ ages of analyzed baddeleyite and zircon grains. Filled bars indicate analyses that are used for the calculation of the mean age. Age errors are shown as x/y/z (internal only / internal + spike calibration / internal + spike calibration + decay constant errors).

tinct magmatic episodes (Fig. 1). In all samples, baddeleyite and zircon grains were small, below 150 μm along the c-axis.

Uranium-lead age determinations using chemical abrasion, isotope-dilution thermal ionization mass spectrometry (CA-ID-TIMS) techniques were conducted following the standard laboratory techniques of the Department of Earth Sciences at the University of Geneva (Switzerland) which are described in more detail elsewhere (Baresel et al., 2017; Davies et al., 2017). Briefly, chemical abrasion (CA) of zircon grains included their annealing at 900 °C for ~48 h and subsequent partial dissolution in HF and trace HNO_3 at 180 °C for 15 h in Parr bombs. The abraded zircon crystals were transferred into 3 ml Savillex beakers, and washed, first in 6 M HCl to remove adsorbed Pb after CA and then subsequently several times with 3 M HNO_3. The chemically abraded zircon grains were then loaded into 200 μl Savillex microcapsules, spiked with EARTHTIME ^{202}Pb-^{205}Pb-^{233}U-^{235}U tracer solution (ET2535) (Condon et al., 2015) and dissolved in ~70 μl 40% HF at 210 °C for 48 h. Subsequently, the samples were converted into chloride form, dried down again and re-dissolved in 3 M HCl for ion-exchange chromatography. A single column anion exchange chemistry was used to separate U and Pb from matrix elements (Krogh, 1973). The U and Pb fractions were combined, dried down and loaded on out-gassed Re-filaments with a Si-Gel emitter (Gerstenberger & Haase, 1997). In contrast to zircon grains, baddeleyite grains were cleaned multiple times in 0.3 M HNO_3 prior to addition of ET2535 spike solution and digestion in Parr bombs. The ion-exchange chromatography separation of U and Pb was identical to that used for the zircon grains.

Measurements of U and Pb isotopes were conducted either on a Thermo Scientific Triton or an IsotopX Phoenix thermal ionization mass spectrometer installed at the Department of Earth Sciences of the University of Geneva. Lead isotope measurements on the Triton were done in dynamic mode on a MasCom secondary electron multiplier, on the Phoenix an axial ion-counting Daly photomultiplier was used. On both mass spectrometers, U isotopes were measured in oxide form (i.e. UO_2) in static mode on Faraday cups equipped with $10^{12}\Omega$ resistors. The U isotopic ratios were corrected for isobaric interferences of $^{233}U^{18}O^{16}O$ on $^{235}U^{16}O_2$ using an $^{18}O/^{16}O$ ratio of 0.00205. The EARTHTIME U and Pb double-isotope (^{202}Pb-^{205}Pb-^{233}U-^{235}U) spike was used to correct for instrumental U and Pb isotope fractionation (Condon et al., 2015). We assumed that all common Pb originates from laboratory blank with an isotopic composition equal to $^{206}Pb/^{204}Pb = 17.100 \pm 0.205$ (1σ); $^{207}Pb/^{204}Pb = 15.150 \pm 0.105$ (1σ); $^{208}Pb/^{204}Pb = 36.17 \pm 0.253$ (1σ). Data reduction was performed using Tripoli and Redux software (Bowring et al., 2011). All results are presented as $^{206}Pb/^{238}U$ dates (Fig. 2), corrected for initial ^{230}Th-^{238}U disequilibrium by assuming a constant partitioning relationship between the zircon (or baddeleyite) and melt of 0.2, however, this correction has almost no impact on calculated baddeleyite ages as they contain almost no Th. The uncertainties are provided in the x/y/z format (analytical error / spike calibration + analytical error / decay constant + spike calibration + analytical error); in the text, only x-errors are reported except when directly compared with $^{40}Ar/^{39}Ar$ or astrochronological data that is not calibrated relative to U-Pb ages.

3.2. Bulk grain solution Hf isotope measurements made using a MC-ICP-MS

Three to five zircon or baddeleyite grains from each sample were analyzed for their Hf isotopic compositions. Also, Hf isotopes were measured from three zircon grains from sample SA39, which was previously dated in Sell et al. (2014). Sample SA39 is a granophyre sill from the central Lebombo (see Fig. 1) and its emplacement age is interpreted to be 181.31 ± 0.19 Ma (Sell et al., 2014). Hafnium isotopic analysis followed the published methodology from the Geneva lab (D'Abzac et al., 2016; Farina et al., 2018). Briefly, Hf was isolated from matrix elements through an ion-exchange column chromatography adopted from a published protocol (Augland & David, 2015), using the wash-out of the column chromatography that was used to isolate U and Pb. After column chemistry, the Hf cut was dried and re-dissolved in a 0.3 M HNO_3 + 0.005 M HF solution for analysis on a Thermo Scientific Neptune Plus multi-collector inductively coupled plasma mass spectrometer (MC-ICP-MS) at the Department of Earth Sciences of the University of Geneva. The cup configuration of the mass spectrometer was adjusted to measure the isotopes ^{172}Yb, ^{173}Yb, ^{175}Lu, ^{176}Hf, ^{177}Hf, ^{178}Hf, ^{179}Hf, ^{180}Hf and ^{181}Ta simultaneously in low resolution mode. During each analytical session, several Plešovice and JMC475 Hf standard solutions were analyzed together with the zircon and baddeleyite samples. Data reduction to obtain the $^{176}Hf/^{177}Hf$ ratio of a zircon or baddeleyite included on peak zero baseline correction, correction for mass bias induced by the mass spectrometer, correction of isobaric interferences of ^{176}Lu and ^{176}Yb on ^{176}Hf and an offset correction by adjusting the $^{176}Hf/^{177}Hf$ ratio of the sample for the observed difference between the measured and preferred value of the JMC475 Hf standard (i.e. 0.282160) (Nowell et al., 1998). More details on measurement protocol and data reduction are given in supplementary material of Farina et al. (2018). Data is presented as initial εHf values using a present-day CHUR composition of $^{176}Hf/^{177}Hf_{CHUR} = 0.282785$ and $^{176}Lu/^{177}Hf_{CHUR} = 0.0336$ (Bouvier et al., 2008), a ^{176}Lu decay constant ($\lambda^{176}Lu$) of 1.867×10^{-11} year^{-1} (Scherer et al., 2001) and the sample age equals our recommended emplacement age (see Table S5). The uncertainty on a single measurement is estimated to 1.5 εHf units (2SD) based on the reproducibility of several measurements of Plešovice zircon during the same analytical session as the unknowns. The average $^{176}Hf/^{177}Hf$ ratio of all measured Plešovice solutions is 0.28248 ± 4, which translates to a εHf value of −3.3 ± 1.5 (2SD) at an age of 336.79 Ma (Widmann et al., 2019). This is identical to the published value of εHf = −3.3 ± 0.5 (Sláma et al., 2008). For further data quality control and to check if instrumental mass fractionation was accurately corrected for, we also report the ratios of the stable Hf isotopes $^{178}Hf/^{177}Hf$ and $^{180}Hf/^{177}Hf$ (Spencer et al., 2020). All, except two samples have $^{178}Hf/^{177}Hf$ and $^{180}Hf/^{177}Hf$ ratios within ± 200 ppm of the recommended values and therefore pass the quality test as suggested by Spencer et al. (2020). However, the two grains with a larger offset (SA100_Bd6b and Z49_z7, see Table S6) have εHf values that are within error identical to the other grains of their respective sample and are therefore included in the discussion.

4. Results

Zircon CA-ID-TIMS U-Pb ages, baddeleyite ID-TIMS U-Pb ages and Hf isotopic compositions are presented in supplementary Tables S5 and

S6, the weighted means and concordia plots are shown in Fig. 2 and S1. Most of the ID-TIMS U-Pb ages of baddeleyite from samples SA100 and SA102 from the Karoo basin are concordant within uncertainty (6 of 8 and 8 of 10 for SA100 and SA102, respectively). The discordancy however, is mostly the result of the assumed blank $^{207}Pb/^{204}Pb$ ratio and its associated error, which has no impact on the calculated $^{206}Pb/^{238}U$ ages. Individual baddeleyite ages range from 183.50 to 182.78 Ma for SA100 and from 183.74 to 180.07 Ma for SA102. The complex age spectra of these samples are likely because baddeleyite grains are not amenable to chemical abrasion, which is used to remove the effects of secondary Pb-loss (Rioux et al. 2010). Therefore, it is likely that some of the age scatter in samples SA100 and SA102 has been caused by unmitigated Pb-loss, leading to artificially young ages (see, e.g., Schaltegger & Davies, 2017). The emplacement ages of 183.33 ± 0.11 Ma (MSWD = 2.7; n = 3) and 183.36 ± 0.17 Ma (MSWD = 0.9; n = 4) for samples SA100 and SA102 respectively, are thus constructed using the weighted average of the oldest baddeleyite clusters in each sample.

Samples SA91 and Z49 yielded zircon with relatively simple age spectra and the Th-corrected weighted mean $^{206}Pb/^{238}U$ ages center around 183.04 Ma (MSWD = 4.2; n = 3) and 176.78 Ma (MSWD = 5.2; n = 5), respectively. These slightly elevated MSWD values indicate some excess scatter in the calculated ages beyond analytical uncertainty, either due to a non-complete removal of Pb-loss (too young ages) or small xenocrystic cores (too old ages). For sample SA91, omitting the oldest or youngest zircon does not result in a significant change in the average and we therefore prefer to use all ages to estimate its time of emplacement of 183.04 ± 0.07 Ma. Regarding sample Z49, the youngest age deviates the most from the mean value, suggesting that this zircon still contained unmitigated Pb-loss. Omitting this age from calculations gives an average of 176.84 ± 0.06 Ma and a MSWD = 2.1 (n = 4), which is our preferred age for sample Z49. We note however, that our choice of zircon analysis to include in the weighted mean age of rock Z49 does not influence our subsequent interpretations.

Zircon grains from the porphyritic rhyolite sample MK492 were very difficult to date due to their extremely low U concentrations, which resulted in almost non-detectable, femtogram amounts of radiogenic Pb. Thus, only 4 out of 24 analyzed zircon grains allowed an age calculation and these ages show a large spread from 184.05 ± 1.59 to 180.42 ± 0.47 Ma. We treated some zircon grains with shorter chemical abrasion of only 6 h to obtain more measurable radiogenic Pb. However, even using short chemical abrasion times only resulted in one grain out of 11 (MK_492_z6) producing interpretable data, and its resulting age is within the range of the other three dated zircon grains that were treated with 15 h of chemical abrasion.

For all samples, εHf values of different grains from the same sample overlap within uncertainty, with the exception of one baddeleyite grain from sample SA100 that has a slightly lower εHf signature than the rest from that sample (Fig. 3, Table S6). The average εHf values of samples from the Karoo basin and the Lebombo are all close to chondritic uniform reservoir (CHUR), and the two oldest samples have the lightest compositions with εHf averages of −1.6 ± 1.6 (2SD; SA100, omitting the one data point at −4.0) and −1.9 ± 1.3 (2SD; SA102). The third Karoo basin sample (SA91) and the two samples from Lebombo (SA39, MK492) have average εHf values between 2.5 ± 1.0 and 3.0 ± 2.0 (2SD). In contrast to all the Karoo basin and Lebombo rocks, the sample Z49 from the Mwenezi monocline has a very distinct, isotopically light mean εHf value of −11.3 ± 1.1 (2SD). Hafnium isotope data from samples SA91, SA39 and Z49 were measured from different zircon than those dated.

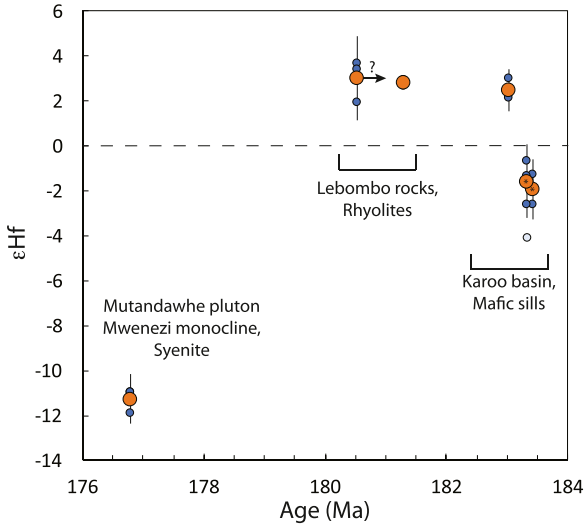

Fig. 3. Hafnium isotopic compositions (given as εHf) of zircon and baddeleyite (indicated with *) grains vs. the estimated age of their host rock (see supplementary Tables S5 and S6) from Karoo-LIP rocks. Small blue dots are individual grains; orange large dots are mean values ± 2SD. One individual zircon grain, shown as a pale blue dot, has been omitted for calculations. Arrow with question mark illustrates that the age of sample MK492 is uncertain and could be older than 180.42 ± 0.47 Ma (see text for further discussion).

5. Discussion

5.1. New ages for Karoo magmatism

Three new ages are presented for the sill complex in the Karoo basin (i.e. SA91, SA100 and SA102) which were emplaced over a very short time interval between 183.04 ± 0.07 and 183.36 ± 0.17 Ma. This contrasts with the newly determined age of sample Z49 from the Mwenezi area of 176.84 ± 0.06 Ma, which represents the youngest high-precision U-Pb age determined so far from the Karoo-LIP.

As mentioned previously, zircon grains from the Lebombo rhyolite MK492 are difficult to date due to their very low U and radiogenic Pb concentrations. The four zircon grains that were datable (out of 24 attempts) exhibit a large spread in Th-corrected $^{206}Pb/^{238}U$ ages from 184.1 ± 1.6 to 180.42 ± 0.47 Ma. An accurate estimate of its emplacement age is therefore difficult. The observed age spread could derive from Pb-loss, however, radiation damage to the crystal lattice is likely limited due to the very low U concentrations of these zircon grains. Furthermore, treating zircon from sample MK492 with a shorter chemical abrasion did not result in a different age, suggesting that it is unlikely that the age spread is entirely due to Pb-loss. One granophyre sill (SA39) and one other rhyolite (SA152) close to sample MK492 were dated via CA-ID-TIMS U-Pb by Sell et al. (2014), and zircon grains from both these rocks also show excess scatter (1.5 to 2.0 Ma age variation). Sell et al. (2014) argued that the youngest zircon ages are representative for the emplacement of the sills (SA39 = 181.31 ± 0.19 Ma and SA152 = 179.32 ± 0.18 Ma), meaning that older grains reflect either antecrystic or xenocrystic zircon grains. The individual zircon grains for Lebombo sample MK492 have Hf isotopic compositions within error, with overlapping εHf values from 1.9 ± 1.5 to 3.7 ± 1.5 (2SD) (supplementary Table S6). However, $^{206}Pb/^{238}U$ ages and εHf values of these grains correlate negatively, meaning that the oldest zircon grain (i.e. 184.1 ± 1.6 Ma) has the lowest Hf isotopic composition. This could hint to the fact that zircon grains in these rocks may contain small, resorbed cores with low εHf, for example from the melting of a gabbroic precursor (Miller & Harris, 2007) or inherited from crustal contamination. Especially regarding the very low U concentrations of zircon from sample MK492, very small amounts of inherited cores could strongly bias the calculated age. This would suggest that the younger zircon ages of sample MK492 (180.4 to 182.1 Ma) might be closest to the time of its emplacement.

However, given the precision on the Hf isotope analyses used to argue for the existence of small inherited zircon in sample MK492, this hypothesis remains speculative and the origin of the variable zircon ages

in the three analyzed silicic rocks from the Lebombo (this study and Sell et al., 2014) remain enigmatic.

5.2. Timing of Karoo and Ferrar LIPs magmatism

Based on $^{40}Ar/^{39}Ar$ ages, it has been suggested that Karoo-LIP magmatism started at ~185 Ma in the Karoo basin (Jourdan et al., 2008) and ended with the intrusion of felsic plutons around 174 Ma (Jourdan et al., 2005) in the Mwenezi region (Fig. 1), and that the magmatic activity was relatively continuous over almost 13 Ma, with a peak period lasting ~4.5 Ma between 184.0 and 179.5 Ma (Jourdan et al., 2008). Based on a more stringent selection criteria and retaining only true plateau ages with >70% of ^{39}Ar released, recalculating all $^{40}Ar/^{39}Ar$ ages using the decay constants of Renne et al. (2011) (see Table S2 for updated $^{40}Ar/^{39}Ar$ ages), these age data rather suggest that the duration of the magmatism (including silicic intrusions) was spread from ca. 185 Ma to 176 Ma with the bulk of the magmatism erupting or intruding from 183.20 ± 0.67 Ma to 182.84 ± 0.72 Ma in the southern province (Karoo basin and Lesotho basalt pile) and from 180.53 ± 0.75 Ma to 180.92 ± 0.36 Ma in the northern province (Shadi-Shadi and Okavango dike swarm; Fig. 1, Table S2 and see also Ware et al., 2018). This ends in a revised duration of the main magmatic pulses of the Karoo-LIP to ca. 3 to 3.5 Ma, and following Ware et al. (2018), the Karoo basin magmatic event likely took place in less than a million year. However, assessing the true duration of the sill emplacement into the Karoo basin is not possible using the $^{40}Ar/^{39}Ar$ data set since the age resolution is too low. Combining our new and published U-Pb zircon and baddeleyite ages (n = 20 samples; including data from Burgess et al., 2015; Sell et al., 2014 and Corfu et al., 2016) from the Karoo basin sill complex, results in a U-Pb dataset that is in agreement with the reinterpreted $^{40}Ar/^{39}Ar$ data set, in particular when all sources of errors are included for both $^{40}Ar/^{39}Ar$ and U-Pb ages. The U-Pb ages are significantly more precise, with all weighted mean ages differing by less than 700′000 years. The slightly less precise U-Pb ages from Corfu et al. (2016) are generally a bit younger compared to those from Burgess et al. (2015), Sell et al. (2014) and our new ages. If these less precise ages of Corfu et al. (2016) are excluded, the rocks from the Karoo basin magmatic event range from 183.36 ± 0.17 to 183.04 ± 0.07 Ma, suggesting that the event had a duration of 320 ± 180 ky and peaked at ca. 183.2 Ma (Fig. 4). Our new data also support the hypothesis that the sill complex of the Karoo basin and the extrusive and intrusive rocks of the Ferrar-LIP were two isolated, temporally distinct, short-pulsed magmatic events separated by approximately 460′000 years, in agreement with Burgess et al. (2015) (Fig. 4).

Northeast of the Karoo basin is the Lebombo monocline, a magmatic complex that is also associated with the Karoo-LIP. The Lebombo monocline is a N-S striking tectonic feature that contains basaltic (e.g. Sabie River Basalt Fm) and silicic volcanic rocks (e.g. Jozini Ryholites), as well as intrusive rocks (Bristow, 1982 and Sweeney et al., 1994) (Fig. 1). Due to its N-S orientation and lithological diversity, the Lebombo monocline is interpreted to be a volcanic rifted margin that developed due to progressive lithospheric extension that preceded the breakup of Gondwana (Bristow, 1982; Klausen, 2009). Sample MK492 is a porphyritic rhyolite flow collected in the central part of the Lebombo and as discussed previously, it is difficult to accurately estimate its eruption age. The youngest zircon age obtained from sample MK492 (180.42 ± 0.47 Ma) agrees with other published U-Pb ages from this location (e.g. SHRIMP data from Riley et al., 2004 or sample SA152 from Sell et al., 2014) and a recalculated $^{40}Ar/^{39}Ar$ age of 179.6 ± 0.7 Ma on sample SA2 Jozini Rhyolite obtained by Jourdan et al. (2007b) and thus, likely approximates the emplacement age of MK492. Taking the measured εHf values into account shows that the sample averages for the Karoo basin (SA102, SA100 and SA91) and Lebombo (MK492, SA39) rocks range from −1.9 ± 1.3 to 3.0 ± 1.9 (2SD) (Fig. 3). The εHf values for the oldest two Karoo basin sills are the lightest (−1.9 and −1.6) while those for the youngest sill and the two Lebombo samples plot between 2.5 and 3.0. This could

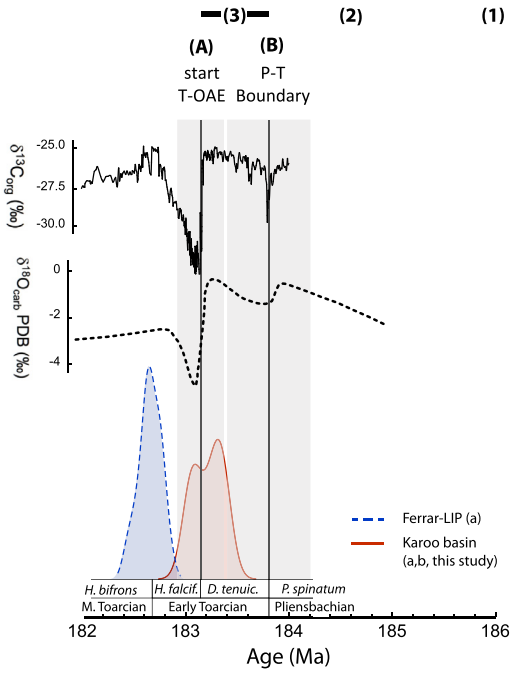

Fig. 4. Carbon and oxygen isotope trends in sediments across the Pliensbachian-Toarcian (P-T) boundary and the Toarcian oceanic anoxic event (T-OAE) combined with the probability density distribution of high-precision U-Pb ages for Ferrar-LIP rocks and sill complex in the Karoo basin. Magmatism associated with these two events occurred over short time intervals and around 460′000 years apart. (1), (2) and (3) are the oldest three of six extinction events in the late Pliensbachian to early Toarcian following Caruthers et al. (2013). (A) and (B) illustrate the extinction pulses over the P-T boundary (Dera et al., 2010) and at the beginning of the T-OAE (Joral et al., 2011). Age of P-T boundary and T-OAE are from Ruhl et al. (2016) and Sell et al. (2014), respectively. While magmatism of the Karoo basin sill complex occurs contemporaneously with the T-OAE suggesting causality between these two events, it postdates earlier extinction pulses and thus cannot be their trigger. a: Burgess et al. (2015), b: Sell et al. (2014). Oxygen isotope trend is an estimated average value after Korte et al. (2015) and C isotope curve is from Ruebsam et al. (2019). Ammonite zones in *italic* are after Sell et al. (2014); tenuic. is tenuicostatum and falcif. is falciferum.

indicate that earliest sills in the Karoo basin were slightly more contaminated with continental crust or that the two groups tapped two mantle reservoirs with slightly different Hf isotopic compositions. The fact that the two silicic samples from the Lebombo have identical εHf values as sill SA91 from the Karoo basin suggests that they have a similar mantle source. This would also indicate that the two silicic Lebombo rocks were partial melts of basaltic or gabbroic precursors (Miller & Harris, 2007), or highly fractionated leftovers of juvenile mafic magmas (Melluso et al., 2008). While no Hf isotope data is currently available for the basaltic rocks in the central Lebombo, published εNd values range between 3.6 and −2.4 (Sweeney et al., 1994) and thus support the suggested petrogenetic connection between the mafic and silicic Lebombo rocks.

The age of the Mutandawhe pluton (determined from sample Z49), which is found in the SW-NE Mwenezi monocline (located North-East of the Lebombo monocline), is 176.84 ± 0.06/0.20 Ma (see Figs. 1 and 3) and statistically indistinguishable from, yet one order of magnitude more precise than the $^{40}Ar/^{39}Ar$ age of the same sample (176.2 ± 0.7/0.9 Ma; Jourdan et al., 2007b, Table S2), especially taking into account that the $^{40}Ar/^{39}Ar$ system of the amphibole dated recorded a cooling age below ca. 450 °C rather than a crystallization age. Our data, in conjunction with previously published data (Jourdan et al., 2007b) show that the magmatism in the Lebombo – Mwenezi area occurred over more than 3 Ma, which is in stark contrast to the brief and episodic volcanic and intrusive magmatism in the Karoo basin (and the Ferrar-LIP). The εHf values of the zircon grains from the Mutandawhe

pluton are much more negative (−11.3 ± 1.1, 2SD) than the mafic rocks of the Karoo basin and the silicic rocks from the Lebombo, but resemble those of undated but potentially Karoo-LIP associated picrites in the same area; Kamenetsky et al. (2017) published a Hf isotope value of 0.282391 for the latter, which translates to an εHf of −10.0 at 177 Ma, and Jourdan et al. (2007a) report εHf values between −7.2 and −8.1. The Mutandawhe pluton, as well as the picrites, therefore require a distinct melt source or melting processes which either includes reworking of old continental material or a long-term enriched mantle source, very different to what generated the older Karoo rocks. The latter explanation has been favored due to the presence of olivine and pyroxene in the picrites with oxygen isotopic compositions (δ^{18}O) up to 1.5 ‰ heavier than typical mantle derived magmas (Harris et al., 2015). Harris et al. (2015) argue that such heavy δ^{18}O values in primitive rocks like picrites are difficult to explain by crustal contamination, as this would have lowered the MgO and increased the SiO_2 concentration outside of what is observed (SiO_2 = 51 to 52 wt%; MgO = 14.4 to 15.2 wt%). The involvement of a source with heterogeneous radiogenic and stable isotopes, likely metasomatically modified mantle lithosphere, has often been used as explanation for the observed various geochemical signatures found in Karoo-LIP rocks, including major and trace element concentrations as well as water content (Jourdan et al., 2007a; Ware et al., 2018).

In summary, in agreement with earlier studies, our data show that the Karoo basin magmatic event and the magmatism in the Lebombo-Mwenezi area are distinct in age and duration. The Karoo basin magmatic event was short-lived, and produced a relatively geochemically homogeneous rock assemblage. In contrast, rocks in the Lebombo-Mwenezi monoclines were produced over a protracted time, and they are chemically and isotopically heterogeneous, involving melts from significantly different mantle domains. These differences could also imply that the mechanisms causing the magmatism between these two events were distinct. Further high-precision dating is required to answer this question, with a focus on the age of the magmatism in the central and southern parts of the Lebombo monocline and the age of the picrites. For example, the light Hf isotopic compositions of picrites from the Lebombo and the Mutandawhe pluton suggest some petrochemical connection between the two, but their temporal relationship is unknown. Regarding the short-pulsed magmatic activity of the sill complex in the Karoo basin and the Ferrar-LIP, the magmatism in the central and southern Lebombo and in the Mwenezi area might be individual, relatively short-pulsed events as well. For example, when updating the available recalculated ^{40}Ar/^{39}Ar ages of the Mwenezi area (Jourdan et al., 2007b; Ware et al., 2018) with our more precise U-Pb age of sample Z49 and considering only the ^{40}Ar/^{39}Ar ages with uncertainties ≤ 0.8 Ma for best comparison, all samples fall into a rather short age range of between 176.8 ± 0.1 and 179.0 ± 0.8 Ma (Table S2; Mwenezi, Nuanetsi intrusives) suggesting an apparent duration of 1.2 ± 0.8 Ma. Improving on the high-temporal resolution of the magmatic pulses that occurred over a LIPs lifetime will allow us to better understand the mechanisms of its emplacement and this is also crucial when investigating the connection between LIP magmatism and environmental perturbations.

5.3. The Karoo-Ferrar magmatic events and their relation to Pliensbachian and early Toarcian environmental perturbations

Currently, six extinction pulses of marine nekton are described in literature that occurred in the time period from ~186 to 178 Ma, with the largest drop in diversity occurring over the Pliensbachian-Toarcian boundary with the disappearance of 70 to 90% of the ammonite taxa (Caruthers et al., 2013; Dera et al., 2010). The Pliensbachian-Toarcian boundary extinction event pre-dates a major negative carbon isotope excursion of around −6‰ found in the global sediment record, starting in the Tenuicostatum zone and extending into the Falciferum zone of the early Toarcian (i.e. the Toarcian Oceanic Anoxic Event; T-OAE, Fig. 4) (Hesselbo et al., 2000). At the beginning of the T-OAE, there was an additional extinction pulse that mainly affected benthic foraminifera and brachiopods (Danise et al., 2015; Joral et al., 2011). Due to their rough temporal correlation, the Karoo and Ferrar magmatic events have been deemed responsible for the diverse extinction pulses that occurred from the late Pliensbachian to the middle Toarcian as well as for the T-OAE and its associated environmental perturbations (Caruthers et al., 2013; Schöllhorn et al., 2020).

The Pliensbachian-Toarcian extinction event pre-dates the T-OAE. Based on dated tephra-layers interbedded with ammonite-bearing carbonates from south Peru it has been shown that the age of the Pliensbachian-Toarcian boundary is older than 183.5 Ma and that the T-OAE started after 183.22 ± 0.25 Ma (Sell et al., 2014). In agreement with this estimate, the age of the Pliensbachian-Toarcian boundary has been dated to 183.8 ± 0.4 Ma by astronomical constraints (Ruhl et al., 2016). Out of the 47 rocks dated by U-Pb using high-precision ID-TIMS techniques from the Karoo and Ferrar LIPs (Burgess et al., 2015; Ivanov et al., 2017; Sell et al., 2014; Svensen et al., 2012), the oldest rock has an age of 183.36 ± 0.17/0.27 Ma (± 0.27 Ma incl. all sources of uncertainties for comparison) and thus only overlaps at the margins of the errors with the age of the Pliensbachian-Toarcian boundary (183.8 ± 0.4 Ma). We therefore argue that based on evidence from high-precision geochronology it is unlikely that the Karoo and Ferrar LIPs triggered the biotic crises and environmental perturbations that occurred at the Pliensbachian-Toarcian boundary and before (see also De Lena et al., 2019). On the other hand, the age of the T-OAE (i.e. 183.22 ± 0.25 Ma; Sell et al., 2014) correlates temporally with the age of the sill complex that intruded the Karoo basin, which may point to causality between these two events (Fig. 4). The Karoo basin hosts sediments rich in organic material and intrusion of sills into these sediments likely released large amounts of thermogenic CO_2 and methane, which can cause a global warming and a biotic crisis (Aarnes et al., 2010, 2011; Svensen et al., 2012). In concert with the T-OAE, oxygen isotopic compositions from belemnite and other marine calcite fossils, which can be used as proxy for seawater palaeotemperatures, also shifted towards lighter values, i.e. warmer temperatures (Korte et al., 2015). The absence of a large volcanic eruption before the T-OAE might explain why oxygen isotopes are rather constant in calcic fossils until this event, implying that cold temperatures governed from the late Pliensbachian until the middle Tenuicostatum zone (Gómez et al., 2016; Korte et al., 2015). We therefore support the idea that the strong environmental perturbations, as evident by the large drop in $\delta^{13}C_{org}$ and $\delta^{18}O_{carb}$ of marine sediments, marking the “early Toarcian super warming” were a consequence of the onset of the Karoo magmatism and, notably, the intrusion of sills into the Karoo basin (Svensen et al., 2012; Gómez et al., 2016; Korte et al., 2015; Ruebsam et al., 2019) (Fig. 4). Nevertheless, there are two caveats to this conclusion. First, the lower parts of the Lebombo monocline, such as the Mashikiri nephelinites predate the basaltic lava flows (Sweeney et al., 1994) and could be older than the Karoo basin sills, but they currently remain undated and secondly, almost no high-precision data exists to accurately and precisely constrain the ages of the Pliensbachian-Toarcian boundary and the T-OAE (i.e. Sell et al., 2014 gives an age for the T-OAE, but only a minimum age for the boundary). Further high-precision dating of Karoo-LIP rocks and the stratigraphic records is therefore required to confirm the connection between the Karoo magmatic event and the observed shift in the climate during the early Toarcian suggested here.

6. Conclusions

This study presents new U-Pb (CA)-ID-TIMS dates and εHf values of baddeleyeite and zircon grains from mafic and felsic rocks of the Karoo-LIP. We combine the U-Pb data with a compiled ^{40}Ar/^{39}Ar age database of Karoo rocks that has been filtered for true plateau ages with >70% of ^{39}Ar released and in which all ^{40}Ar/^{39}Ar ages are recalculated using current best estimates of the decay constants. The updated ^{40}Ar/^{39}Ar and high-precision U-Pb ages correspond well and suggest that major episodes of the emplacement of the Karoo-LIP happened in

distinct pulses. We confirm that the sill complex, which intruded into the Karoo basin was emplaced over a short-lived event (320 ± 180 ka) and occurred between ca. 183.4 and 183.0 Ma, and therefore predates the magmatism in the Ferrar-LIP by around 460 ka. The first high-precision U-Pb age of 176.84 ± 0.06 Ma of the late stage felsic rocks in the northern part of the Mwenezi monocline (Mutandawhe pluton) confirms that the Karoo-LIP magmatism took place over a protracted period, and likely ended around 6.5 Ma later than the Karoo basin magmatic event. Based on high-precision data, the onset of the Karoo-LIP magmatism seems to have occurred around 183.36 ± 0.17 Ma and likely postdates the extinction pulses at the Pliensbachian-Toarcian boundary although some part of the Karoo LIP remains undated (e.g., Mashikiri nephelinites) and might be older. Nevertheless, this age agrees with the onset of the T-OAE event. We thus support the idea that Karoo-LIP magmatism caused the T-OAE and eventually also the contemporaneous early Toarcian warming.

Declaration of Competing Interest

The authors declare no conflict of interest.

Acknowledgments

This work was supported by the Swiss National Science Foundation (project numbers 181172, 182007 and 162341) to NDG and US. We thank Christopher Spencer and an anonymous reviewer for their constructive criticism and Marc-Alban Millet for editorial handling of the manuscript.

Supplementary materials

Supplementary material associated with this article can be found, in the online version, at doi:10.1016/j.ringeo.2020.100005.

References

Aarnes, I., Svensen, H., Connolly, J. A. D., & Podladchikov, Y. Y. (2010). How contact metamorphism can trigger global climate changes: Modeling gas generation around igneous sills in sedimentary basins. *Geochimica et Cosmochimica Acta, 74*(24), 7179–7195. 10.1016/j.gca.2010.09.011.

Aarnes, I., Svensen, H., Polteau, S., & Planke, S. (2011). Contact metamorphic devolatilization of shales in the Karoo Basin, South Africa, and the effects of multiple sill intrusions. *Chemical Geology, 281*(3-4), 181–194. 10.1016/j.chemgeo.2010.12.007.

Augland, L. E., & David, J. (2015). Protocrustal evolution of the Nuvvuagittuq Supracrustal Belt as determined by high precision zircon Lu–Hf and U–Pb isotope data. *Earth and Planetary Science Letters, 428*, 162–171. 10.1016/j.epsl.2015.07.039.

Baresel, B., Bucher, H., Brosse, M., Cordey, F., Guodun, K., & Schaltegger, U. (2017). Precise age for the Permian-Triassic boundary in South China from high-precision U-Pb geochronology and Bayesian age-depth modeling. *Solid Earth, 8*(2), 361–378. 10.5194/se-8-361-2017.

Bouvier, A., Vervoort, J. D., & Patchett, P. J. (2008). The Lu–Hf and Sm–Nd isotopic composition of CHUR: Constraints from unequilibrated chondrites and implications for the bulk composition of terrestrial planets. *Earth and Planetary Science Letters, 273*(1-2), 48–57. 10.1016/j.epsl.2008.06.010.

Bowring, J. F., McLean, N. M., & Bowring, S. A. (2011). Engineering cyber infrastructure for U-Pb geochronology: Tripoli and U-Pb_Redux. *Geochemistry Geophysics Geosystems, 12*(6). 10.1029/2010GC003479.

Bristow, J. W. (1982). Geology and structure of Karoo volcanic and sedimentary rocks of the northern and central Lebombo (South Africa). *Transactions - Geological Society of South Africa, 85*(3), 167–178.

Bryan, S. E., & Ernst, R. E. (2008). Revised definition of Large Igneous Provinces (LIPs). *Earth-Science Reviews, 86*(1-4), 175–202. 10.1016/j.earscirev.2007.08.008.

Burgess, S. D., Bowring, S. A., Fleming, T. H., & Elliot, D. H. (2015). High-precision geochronology links the Ferrar large igneous province with early-Jurassic ocean anoxia and biotic crisis. *Earth and Planetary Science Letters, 415*, 90–99. 10.1016/j.epsl.2015.01.037.

Burgess, S. D., Muirhead, J. D., & Bowring, S. A. (2017). Initial pulse of Siberian Traps sills as the trigger of the end-Permian mass extinction. *Nature Communications*, 1–4. 10.1038/s41467-017-00083-9.

Capriolo, M., Marzoli, A., Aradi, L. E., Callegaro, S., Corso, J. D., Newton, R. J., Mills, B. J. W., Wignall, P. B., Bartoli, O., Baker, D. R., Youbi, N., Remusat, L., Spiess, R., & Szabó, C. (2020). Deep CO_2 in the end-Triassic Central Atlantic Magmatic Province. *Nature Communications*, 1–11. 10.1038/s41467-020-15325-6.

Caruthers, A. H., Smith, P. L., & Gröcke, D. R. (2013). The Pliensbachian–Toarcian (Early Jurassic) extinction, a global multi-phased event. *Palaeogeography, Palaeoclimatology, Palaeoecology, 386*, 104–118. 10.1016/j.palaeo.2013.05.010.

Condon, D. J., Schoene, B., McLean, N. M., Bowring, S. A., & Parrish, R. R. (2015). Metrology and traceability of U-Pb isotope dilution geochronology (EARTH-TIME Tracer Calibration Part I). *Geochimica et Cosmochimica Acta, 164*, 464–480. 10.1016/j.gca.2015.05.026.

Corfu, F., Svensen, H., & Mazzini, A. (2016). Comment to paper: Evaluating the temporal link between the Karoo LIP and climatic–biologic events of the Toarcian Stage with high-precision U–Pb geochronology by Bryan Sell, Maria Ovtcharova, Jean Guex, Annachiara Bartolini, Fred Jourdan, Jorge E. Spangenberg, Jean-Claude Vicente, Urs Schaltegger in Earth and Planetary Science Letters 408 (2014) 48–56. *Earth and Planetary Science Letters, 434*, 349–352. 10.1016/j.epsl.2015.07.010.

D'Abzac, F.-X., Davies, J. H. F. L., Wotzlaw, J.-F., & Schaltegger, U. (2016). Hf isotope analysis of small zircon and baddeleyite grains by conventional multi collector-inductively coupled plasma-mass spectrometry. *Chemical Geology, 433*, 12–23. 10.1016/j.chemgeo.2016.03.025.

Danise, S., Twitchett, R. J., & Little, C. T. S. (2015). Environmental controls on Jurassic marine ecosystems during global warming. *Geology, 43*(3), 263–266. 10.1130/G36390.1.

Davies, J. H. F. L., Marzoli, A., Bertrand, H., Youbi, N., Ernesto, M., & Schaltegger, U. (2017). End-Triassic mass extinction started by intrusive CAMP activity. *Nature Communications, 8*, 1–8. 10.1038/ncomms15596.

De Lena, L. F., Taylor, D., Guex, J., Bartolini, A., Adatte, T., van Acken, D., Spangenberg, J. E., Samankassou, E., Vennemann, T., & Schaltegger, U. (2019). The driving mechanisms of the carbon cycle perturbations in the late Pliensbachian (Early Jurassic). *Scientific Reports*, 1–12. 10.1038/s41598-019-54593-1.

Dera, G., Neige, P., Dommergues, J.-L., Fara, E., Laffont, R., & Pellenard, P. (2010). High-resolution dynamics of Early Jurassic marine extinctions: the case of Pliensbachian–Toarcian ammonites (Cephalopoda). *Journal of the Geological Society, 167*(1), 21–33. 10.1144/0016-76492009-068.

Duncan, R. A., Hooper, P. R., Rehacek, J., Marsh, J., & Duncan, A. R. (1997). The timing and duration of the Karoo igneous event, southern Gondwana. *Journal of Geophysical Research: Solid Earth, 102*(B8), 18127–18138.

Farina, F., Dini, A., Davies, J. H. F. L., Ovtcharova, M., Greber, N. D., Bouvier, A.-S., Baumgartner, L., Ulianov, A., & Schaltegger, U. (2018). Zircon petrochronology reveals the timescale and mechanism of anatectic magma formation. *Earth and Planetary Science Letters, 495*, 213–223. 10.1016/j.epsl.2018.05.021.

Ganino, C., & Arndt, N. (2009). Climate changes caused by degassing of sediments during the emplacement of large igneous provinces. *Geology, 37*(4), 323–326. 10.1130/G25325A.1.

Gerstenberger, H., & Haase, G. (1997). A highly effective emitter substance for mass spectrometric Pb isotope ratio determinations. *Chemical Geology, 136*(3-4), 309–312. 10.1016/S0009-2541(96)00033-2.

Gómez, J. J., Comas-Rengifo, M. J., & Goy, A. (2016). Palaeoclimatic oscillations in the Pliensbachian (Early Jurassic) of the Asturian Basin (Northern Spain). *Climate of the Past, 12*(5), 1199–1214. 10.5194/cp-12-1199-2016.

Gómez, J. J., Goy, A., & Canales, M. L. (2008). Seawater temperature and carbon isotope variations in belemnites linked to mass extinction during the Toarcian (Early Jurassic) in Central and Northern Spain. Comparison with other European sections. *Palaeogeography, Palaeoclimatology, Palaeoecology, 258*(1-2), 28–58. 10.1016/j.palaeo.2007.11.005.

Harris, C., Roux, P., Cochrane, R., Martin, L., Duncan, A. R., Marsh, J. S., Roex, A. P., & Class, C. (2015). The oxygen isotope composition of Karoo and Etendeka picrites: High $\delta^{18}O$ mantle or crustal contamination? *Contributions to Mineralogy and Petrology, 170*(1), 1–24. 10.1007/s00410-015-1164-1.

Heimdal, T. H., Callegaro, S., Svensen, H. H., Jones, M. T., Pereira, E., & Planke, S. (2019). Evidence for magma–evaporite interactions during the emplacement of the Central Atlantic Magmatic Province (CAMP) in Brazil. *Earth and Planetary Science Letters, 506*, 476–492. 10.1016/j.epsl.2018.11.018.

Heimdal, T. H., Jones, M. T., & Svensen, H. H. (2020). Thermogenic carbon release from the Central Atlantic magmatic province caused major end-Triassic carbon cycle perturbations. *Proceedings of the National Academy of Sciences of the United States of America, 117*(22). 10.1073/pnas.2000095117/-/DCSupplemental.

Hesselbo, S. P., Grocke, D. R., Jenkyns, H. C., Bjerrum, C. J., Farrimond, P., Bell, H., & Green, O. R. (2000). Massive dissociation of gas hydrate during a Jurassic oceanic anoxic event. *Nature, 406*(6794), 392–395. 10.1038/35019044.

Ivanov, A. V., Meffre, S., Thompson, J., Corfu, F., Kamenetsky, V. S., Kamenetsky, M. B., & Demonterova, E. I. (2017). Timing and genesis of the Karoo-Ferrar large igneous province: New high precision U-Pb data for Tasmania confirm short duration of the major magmatic pulse. *Chemical Geology, 455*, 32–43. 10.1016/j.chemgeo.2016.10.008.

Jones, D. L., Duncan, R. A., Briden, J. C., Randall, D. E., & MacNiocaill, C. (2001). Age of the Batoka basalts, northern Zimbabwe, and the duration of Karoo Large Igneous Province magmatism. *Geochemistry, Geophysics, Geosystems, 2*(2).

Joral, F. G., Gómez, J. J., & Goy, A. (2011). Mass extinction and recovery of the Early Toarcian (Early Jurassic) brachiopods linked to climate change in Northern and Central Spain. *Palaeogeography, Palaeoclimatology, Palaeoecology, 302*(3-4), 367–380. 10.1016/j.palaeo.2011.01.023.

Jourdan, F., Bertrand, H., Schärer, U., Blichert-Toft, J., Féraud, G., & Kampunzu, A. B. (2007a). Major and Trace Element and Sr, Nd, Hf, and Pb Isotope Compositions of the Karoo Large Igneous Province, Botswana–Zimbabwe: Lithosphere vs Mantle Plume Contribution. *Journal of Petrology, 48*(6), 1043–1077. 10.1093/petrology/egm010.

Jourdan, F., Féraud, G., Bertrand, H., Kampunzu, A. B., Tshoso, G., Le Gall, B., Tiercelin, J. J., & Capiez, P. (2004). The Karoo triple junction questioned: evidence from Jurassic and Proterozoic $^{40}Ar/^{39}Ar$ ages and geochemistry of the giant Okavango dyke swarm (Botswana). *Earth and Planetary Science Letters, 222*(3-4), 989–1006.

Jourdan, F., Féraud, G., Bertrand, H., & Watkeys, M. K. (2007b). From flood basalts to the inception of oceanization: Example from the $^{40}Ar/^{39}Ar$ high-resolution pic-

ture of the Karoo large igneous province. *Geochemistry Geophysics Geosystems, 8*(2). 10.1029/2006GC001392.

Jourdan, F., Féraud, G., Bertrand, H., Kampunzu, A. B., Tshoso, G., Watkeys, M. K., & Le Gall, B. (2005). Karoo large igneous province: Brevity, origin, and relation to mass extinction questioned by new $^{40}Ar/^{39}Ar$ age data. *Geology, 33*(9) 745–4. 10.1130/G21632.1.

Jourdan, F., Féraud, G., Bertrand, H., Watkeys, M. K., & Renne, P. R. (2007c). Distinct brief major events in the Karoo large igneous province clarified by new $^{40}Ar/^{39}Ar$ ages on the Lesotho basalts. *Lithos, 98*(1-4), 195–209.

Jourdan, F., Féraud, G., Bertrand, H., Watkeys, M. K., & Renne, P. R. (2008). The $^{40}Ar/^{39}Ar$ ages of the sill complex of the Karoo large igneous province: Implications for the Pliensbachian-Toarcian climate change. *Geochemistry Geophysics Geosystems, 9*(6). 10.1029/2008GC001994.

Kamenetsky, V. S., Maas, R., Kamenetsky, M. B., Yaxley, G. M., Ehrig, K., Zellmer, G. F., Bindeman, I. N., Sobolev, A. V., Kuzmin, D. V., Ivanov, A. V., Woodhead, J., & Schilling, J.-G. (2017). Multiple mantle sources of continental magmatism: Insights from "high-Ti" picrites of Karoo and other large igneous provinces. *Chemical Geology, 455*, 22–31. 10.1016/j.chemgeo.2016.08.034.

Kasbohm, J., & Schoene, B. (2018). Rapid eruption of the Columbia River flood basalt and correlation with the mid-Miocene climate optimum. *Science Advances, 4*(9). 10.1126/sciadv.aat8223.

Klausen, M. B. (2009). The Lebombo monocline and associated feeder dyke swarm: Diagnostic of a successful and highly volcanic rifted margin? *Tectonophysics, 468*(1-4), 42–62. 10.1016/j.tecto.2008.10.012.

Korte, C., Hesselbo, S. P., Ullmann, C. V., Dietl, G., Ruhl, M., Schweigert, G., & Thibault, N. (2015). Jurassic climate mode governed by ocean gateway. *Nature Communications, 6*(1), 59. 10.1038/ncomms10015.

Krogh, T. E. (1973). A low-contamination method for hydrothermal decomposition of zircon and extraction of U and Pb for isotopic age determinations. *Geochimica et Cosmochimica Acta, 37*(3), 485–494. 10.1016/0016-7037(73)90213-5.

Landoll, J. D., Foland, K. A., & Henderson, C. M. B. (1989). Excess argon in amphiboles from fluid interaction and short intrusion interval at the epizonal Marangudzi complex, Zimbabwe. *Journal of Geophysical Research: Solid Earth, 94*(B4), 4053–4069.

Le Gall, B., Tshoso, G., Jourdan, F., Féraud, G., Bertrand, H., Tiercelin, J. J., Kampunzu, A. B., Modisi, M. P., Dyment, J., & Maia, M. (2002). $^{40}Ar/^{39}Ar$ geochronology and structural data from the giant Okavango and related mafic dyke swarms, Karoo igneous province, northern Botswana. *Earth and Planetary Science Letters, 202*(3-4), 595–606.

Luttinen, A. V. (2018). Bilateral geochemical asymmetry in the Karoo large igneous province. *Scientific Reports, 8*(5223), 1–11. 10.1038/s41598-018-23661-3.

Luttinen, A. V., Heinonen, J. S., Kurhila, M., Jourdan, F., Mänttäri, I., Vuori, S. K., & Huhma, H. (2015). Depleted mantle-sourced CFB magmatism in the Jurassic Africa–Antarctica rift: Petrology and $^{40}Ar/^{39}Ar$ and U/Pb chronology of the Vestfjella dyke swarm, Dronning Maud Land, Antarctica. *Journal of Petrology, 56*(5), 919–952.

Melluso, L., Cucciniello, C., Petrone, C. M., Lustrino, M., Morra, V., Tiepolo, M., & Vasconcelos, L. (2008). Petrology of Karoo volcanic rocks in the southern Lebombo monocline, Mozambique. *Journal of African Earth Sciences, 52*(4-5), 139–151. 10.1016/j.jafrearsci.2008.06.002.

Miller, J. A., & Harris, C. (2007). Petrogenesis of the Swaziland and northern Natal rhyolites of the Lebombo rifted volcanic margin, south east Africa. *Journal of Petrology, 48*(1), 185–218. 10.1093/petrology/egl061.

Moulin, M., Fluteau, F., Courtillot, V., Marsh, J., Delpech, G., Quidelleur, X., & Gérard, M. (2017). Eruptive history of the Karoo lava flows and their impact on early Jurassic environmental change. *Journal of Geophysical Research: Solid Earth, 122*(2), 738–772. 10.1002/2016JB013354.

Nowell, G. M., Kempton, P. D., Noble, S. R., Fitton, J. G., Saunders, A. D., Mahoney, J. J., & Taylor, R. N. (1998). High precision Hf isotope measurements of MORB and OIB by thermal ionisation mass spectrometry: insights into the depleted mantle. *Chemical Geology, 149*(3-4), 211–233. 10.1016/S0009-2541(98)00036-9.

Pálfy, J., & Smith, P. L. (2000). Synchrony between Early Jurassic extinction, oceanic anoxic event, and the Karoo-Ferrar flood basalt volcanism. *Geology, 28*(8), 747–750.

Percival, L. M. E., Witt, M. L. I., Mather, T. A., Hermoso, M., Jenkyns, H. C., Hesselbo, S. P., Al-Suwaidi, A. H., Storm, M. S., Xu, W., & Ruhl, M. (2015). Globally enhanced mercury deposition during the end-Pliensbachian extinction and Toarcian OAE: A link to the Karoo–Ferrar Large Igneous Province. *Earth and Planetary Science Letters, 428*, 267–280. 10.1016/j.epsl.2015.06.064.

Renne, P. R., Balco, G., Ludwig, K. R., Mundil, R., & Min, K. (2011). Response to the comment by W.H. Schwarz et al. on "Joint determination of ^{40}K decay constants and $^{40}Ar^{*}/^{40}K$ for the Fish Canyon sanidine standard, and improved accuracy for $^{40}Ar/^{39}Ar$ geochronology" by P.R. Renne et al. (2010). *Geochimica et Cosmochimica Acta, 75*(17), 5097–5100. 10.1016/j.gca.2011.06.021.

Riley, T. R., Leat, P. T., Curtis, M. L., Millar, I. L., Duncan, R. A., & Fazel, A. (2005). Early-middle Jurassic dolerite dykes from western Dronning Maud Land (Antarctica): Identifying mantle sources in the Karoo large igneous province. *Journal of Petrology, 46*(7), 1489–1524. 10.1093/petrology/egi023.

Riley, T. R., Millar, I. L., Watkeys, M. K., Curtis, M. L., Leat, P. T., Klausen, M. B., & Fanning, C. M. (2004). U-Pb zircon (SHRIMP) ages for the Lebombo rhyolites, South Africa: refining the duration of Karoo volcanism. *Journal of the Geological Society, 161*(4), 547–550. 10.1144/0016-764903-181.

Riley, T. R., Curtis, M. L., Leat, P. T., Watkeys, M. K., Duncan, R. A., Millar, I. L., & Owens, W. H. (2006). Overlap of Karoo and Ferrar magma types in KwaZulu-Natal, South Africa. *Journal of Petrology, 47*(3), 541–566.

Rioux, M., Bowring, S., Dudás, F., & Hanson, R. (2010). Characterizing the U–Pb systematics of baddeleyite through chemical abrasion: application of multi-step digestion methods to baddeleyite geochronology. *Contributions to Mineralogy and Petrology, 160*(5), 777–801. 10.1007/s00410-010-0507-1.

Rita, P., Nätscher, P., Duarte, L. V., Weis, R., & De Baets, K. (2019). Mechanisms and drivers of belemnite body-size dynamics across the Pliensbachian–Toarcian crisis. *Royal Society Open Science, 6*(12) 190494–20. 10.1098/rsos.190494.

Ruebsam, W., Mayer, B., & Schwark, L. (2019). Cryosphere carbon dynamics control early Toarcian global warming and sea level evolution. *Global and Planetary Change, 172*, 440–453. 10.1016/j.gloplacha.2018.11.003.

Ruhl, M., Hesselbo, S. P., Hinnov, L., Jenkyns, H. C., Xu, W., Riding, J. B., Storm, M., Minisini, D., Ullmann, C. V., & Leng, M. J. (2016). Astronomical constraints on the duration of the Early Jurassic Pliensbachian Stage and global climatic fluctuations. *Earth and Planetary Science Letters, 455*, 149–165. 10.1016/j.epsl.2016.08.038.

Schaltegger, U., and Davies, J.H.F.L., 2017, Petrochronology of Zircon and Baddeleyite in Igneous Rocks: Reconstructing Magmatic Processes at High Temporal Resolution, in Reviews in Mineralogy and Geochemistry, vol. 83, p. 297–328, doi:10.2138/rmg.2017.83.10

Scherer, E., Münker, C., & Mezger, K. (2001). Calibration of the lutetium-hafnium clock. *Science, 293*(5530), 683–687. 10.1126/science.1061372.

Schöllhorn, I., Adatte, T., Charbonnier, G., Mattioli, E., Spangenberg, J. E., & Föllmi, K. B. (2020). Pliensbachian environmental perturbations and their potential link with volcanic activity: Swiss and British geochemical records. *Sedimentary Geology, 406*, Article 105665. 10.1016/j.sedgeo.2020.105665.

Sell, B., Ovtcharova, M., Guex, J., Bartolini, A., Jourdan, F., Spangenberg, J. E., Vicente, J.-C., & Schaltegger, U. (2014). Evaluating the temporal link between the Karoo LIP and climatic–biologic events of the Toarcian Stage with high-precision U–Pb geochronology. *Earth and Planetary Science Letters, 408*, 48–56. 10.1016/j.epsl.2014.10.008.

Sláma, J., Košler, J., Condon, D. J., Crowley, J. L., Gerdes, A., Hanchar, J. M., Horstwood, M. S. A., Morris, G. A., Nasdala, L., Norberg, N., Schaltegger, U., Schoene, B., Tubrett, M. N., & Whitehouse, M. J. (2008). Plešovice zircon — A new natural reference material for U–Pb and Hf isotopic microanalysis. *Chemical Geology, 249*(1-2), 1–35. 10.1016/j.chemgeo.2007.11.005.

Sobolev, S. V., Sobolev, A. V., Kuzmin, D. V., Krivolutskaya, N. A., Petrunin, A. G., Arndt, N., Radko, V. A., & Vasiliev, Y. R. (2011). Linking mantle plumes, large igneous provinces and environmental catastrophes. *Nature*, 1–7. 10.1038/nature10385.

Spencer, C. J., Kirkland, C. L., Roberts, N. M. W., Evans, N. J., & Liebmann, J. (2020). Strategies towards robust interpretations of in situ zircon Lu–Hf isotope analyses. *Geoscience Frontiers, 11*(3), 843–853. 10.1016/j.gsf.2019.09.004.

Storey, B. C., Vaughan, A. P. M., & Riley, T. R. (2013). The links between large igneous provinces, continental break-up and environmental change: Evidence reviewed from Antarctica. *Earth and Environmental Science Transactions of the Royal Society of Edinburgh, 104*(1), 17–30. 10.1017/S175569101300011X.

Svensen, H., Corfu, F., Polteau, S., Hammer, Ø., & Planke, S. (2012). Rapid magma emplacement in the Karoo Large Igneous Province. *Earth and Planetary Science Letters, 325-326*, 1–9. 10.1016/j.epsl.2012.01.015.

Sweeney, R. J., & Duncan, A. R. (1994). Geochemistry and petrogenesis of central Lebombo basalts of the Karoo igneous province. *Journal of Petrology, 35*(Part 1), 95–125.

Ware, B., Jourdan, F., Tohver, E., Fernandes, K. G., & Chiaradia, M. (2018). Primary hydrous minerals from the Karoo LIP magmas: Evidence for a hydrated source component. *Earth and Planetary Science Letters, 503*, 181–193. 10.1016/j.epsl.2018.09.017.

Widmann, P., Davies, J. H. F. L., & Schaltegger, U. (2019). Calibrating chemical abrasion_ Its effects on zircon crystal structure, chemical composition and UPb age. *Chemical Geology, 511*, 1–10. 10.1016/j.chemgeo.2019.02.026.

Zhang, X., Luttinen, A. V., Elliot, D. H., Larsson, K., & Foland, K. A. (2003). Early stages of Gondwana breakup: the $^{40}Ar/^{39}Ar$ geochronology of Jurassic basaltic rocks from western Dronning Maud Land, Antarctica, and implications for the timing of magmatic and hydrothermal events. *Journal of Geophysical Research: Solid Earth, 108*(B9).